SPI1$^+$CD68$^+$ macrophages as a biomarker for gastric cancer metastasis: a rationale for combined antiangiogenic and immunotherapy strategies

Guofei Deng,[1,2] Pengliang Wang,[3] Rishun Su,[1,2] Xuezeng Sun,[1,2] Zizhen Wu,[4] Zhangsen Huang,[1,2] Liang Gu,[1,2] Hong Yu,[1,2] Zhenzhen Zhao,[1,2] Yulong He,[1,2,5] Mingyu Huo,[1,2] Changhua Zhang,[1,2] Songcheng Yin ⓘ [1,2]

For numbered affiliations see end of article.

Correspondence to
Dr Songcheng Yin;
ysc19911991@163.com

Dr Changhua Zhang;
zhchangh@mail.sysu.edu.cn

Dr Mingyu Huo;
mingyu9318@163.com

Dr Yulong He;
heyulong@mail.sysu.edu.cn

ABSTRACT

Background Tumor-associated macrophages (TAMs) have been demonstrated to be associated with tumor progression. However, the different subpopulations of TAMs and their roles in gastric cancer (GC) remain poorly understood. This study aims to assess the effects of Spi-1 proto-oncogene (SPI1)$^+$CD68$^+$ TAMs in GC.

Methods The distribution of SPI1$^+$CD68$^+$ TAMs in GC tissue was estimated by immunohistochemistry, immunofluorescence, and flow cytometry. Single-cell transcriptome analysis and multiplex fluorescence immunohistochemistry were applied to explore the role of SPI1$^+$CD68$^+$ TAMs in an immune contexture. SPI1 overexpression or knockdown cells were constructed to evaluate its role in macrophage polarization and angiogenesis in vitro and in vivo. Chromatin immunoprecipitation was used to verify the mechanism of SPI1 transcriptional function. The effect of combined antiangiogenic and immunotherapy was further validated using mouse peritoneal metastasis models.

Results Single-cell transcriptome analysis and immunohistochemistry demonstrated that SPI1 was expressed in macrophages, with a higher enrichment in metastatic lesions than in primary tumors. Higher SPI1$^+$CD68$^+$ TAMs infiltration was associated with poor overall survival. Mechanically, SPI1 promoted the M2-type macrophage polarization. SPI1 could bind to the promoter of vascular endothelial growth factor A and facilitate angiogenesis. Moreover, the level of SPI1$^+$CD68$^+$ TAMs infiltration was closely related to the efficacy of immunotherapy, especially when combined with antiangiogenic therapy.

Conclusions The present study showed that SPI1$^+$CD68$^+$ TAMs are a promising biomarker for predicting prognosis, antiangiogenic drug sensitivity, and combination target of immunotherapy in patients with GC.

WHAT IS ALREADY KNOWN ON THIS TOPIC

⇒ The pivotal role of tumor-associated macrophages (TAMs) in the initiation, progression and metastasis of tumors has been widely recognized in the scientific community. The classification and functional characterization of TAMs subsets remain a significant challenge in the field of immunology.

WHAT THIS STUDY ADDS

⇒ Spi-1 proto-oncogene (SPI1)$^+$CD68$^+$ TAMs emerged as a novel proangiogenic macrophage subtype, driving tumor angiogenesis via vascular endothelial growth factor A secretion and intimately associating with the immunosuppressive microenvironment.

HOW THIS STUDY MIGHT AFFECT RESEARCH, PRACTICE OR POLICY

⇒ SPI1$^+$CD68$^+$ TAMs proved to be a promising metastasis-associated biomarker in gastric cancer, presenting a viable target for combined antiangiogenic and immunotherapy approaches.

INTRODUCTION

Owing to its high incidence and metastatic rate, gastric cancer (GC) remains one of the poorly prognosis malignancies worldwide, with the third highest mortality rate among all tumors.[1 2] Tumor recurrence and metastasis are closely related to immune microenvironment. Tumor metastasis represents a highly intricate and multifaceted biological phenomenon, contingent on a myriad of interrelated factors encompassing plasticity, stress responses, and the establishment of an immunosuppressive microenvironment.[3 4] Consequently, devising effective therapeutic approaches for managing metastatic tumors proves notably more intricate when juxtaposed against the treatment of primary tumors. Tumor-associated macrophages (TAMs) play a pivotal role in affecting tumor biology as an integral component of the immune milieu.[5] However, due to the heterogeneity of the tumor microenvironment (TME) intertumor and intratumor, the function of TAMs varies under different conditions, the traditional M1

and M2 classification cannot fully summarize the role of TAMs. More refined subtypes of TAMs that deserve to be investigated.

Tumor immunotherapy, as a novel approach to the treatment of cancer, has been recognized as a promising addition to conventional cancer therapies such as surgery, radiation therapy, chemotherapy, and targeted therapy.[6 7] Tumor immunotherapy elicits tumor-specific immune responses in the host, either actively or passively, to exert its inhibitory and tumoricidal functions. As a rising star in cancer treatment, immunotherapy, represented by immune checkpoint inhibitors (ICIs), has ushered in a new era in the field of tumor therapy. Several candidate targets have undergone rigorous validation, establishing them as pivotal regulatory nodes with demonstrated effectiveness across diverse cancer types.[8 9] Furthermore, studies have demonstrated that immunotherapy has shown promising effects in the context of metastatic tumors.[10] However, current immune checkpoint therapy predominantly focuses on tumor cells themselves, with limited research on immune checkpoints within the TME. Moreover, the development of immune checkpoints specifically tailored to TAMs is currently lacking.

Spi-1 proto-oncogene (SPI1) is a member of the transcription factor family Ets, which is closely associated with myeloid and B-lymphoid cell differentiation,[11] and it plays a vital role in promoting cell maturation in the hematopoietic system.[12] Moreover, SPI1 regulates the expression of various genes, including those encoding immunoglobulins, receptors, and enzymes that are involved in various biological functions of the body.[13] SPI1 mutations could induce acute myeloid leukemia[14] and regulate selective macrophage polarization in asthma.[15] Recently, it was reported that SPI1 promotes the inflammatory response of macrophages in *Helicobacter pylori*-induced gastritis.[16] Nevertheless, research between SPI1 and TAMs in the GC microenvironment is limited.

In this study, we aimed to explore the role of SPI1⁺CD68⁺ TAMs in GC progression, and identify novel immune checkpoint targets that could be used in TAMs-targeted immunotherapy approaches. We found that SPI1⁺CD68⁺ TAMs were differentially infiltrated in primary and metastatic GC lesions. Patients with more infiltration of SPI1⁺CD68⁺ TAMs demonstrated a higher likelihood of metastasis and worse clinical prognosis. Furthermore, SPI1⁺CD68⁺ TAMs were observed to stimulate tumor angiogenesis through increasing vascular endothelial growth factor A (VEGFA) transcription. Moreover, we found a strong correlation between SPI1⁺CD68⁺ TAMs infiltration and immunotherapy. These findings underscore this specific cell subtype as a predictive biomarker for metastasis detection and pave the way for implementing combined antiangiogenic and immunotherapy strategies in clinical practice.

METHODS

Human tissue samples and clinical information of patients with GC

The training group involved 198 individuals diagnosed with primary gastric carcinoma, who underwent radical gastrectomy at the First Affiliated Hospital, Sun Yat-sen University (Guangzhou, China) between November 2010 and December 2012. Clinicopathological and survival data were retrospectively collected, and GC tissue was subjected to immunohistochemical (IHC) and immunofluorescence analyses. GC tissues were also transformed into cell suspensions for flow cytometry analysis. External validation was conducted using another 115 patients from the biobank of Shanghai Outdo Biotech company. A tissue microarray containing 31 patients with metastasis was employed to assess the difference between metastatic and primary tumors. Protocols were performed in accordance with the Declaration of Helsinki for Human Research.

Sample preparation and single-cell RNA sequencing

Six paired tumor and adjacent non-tumor tissue samples, obtained from three patients who underwent gastrectomy in August 2021 at the First Affiliated Hospital of Sun Yat-sen University (Guangzhou, China), were collected for single-cell RNA sequencing (scRNA-seq) experiments. Written informed consent was obtained from each patient. The clinicopathological information of the included patients was shown in the online supplemental table S1. Tissues were washed twice using phosphate-buffered saline (PBS) briefly and dispatched to Berry Genomics Laboratories (Beijing, China) for singular cell dissociation and subsequent single-cell experiments (10x Genomics, USA). The primary sequencing data generated by 10x Genomics were processed for alignment and quantification through the utilization of the Cell Ranger software package (10x Genomics, V.3.0.2).

Data processing of scRNA-seq

The single-cell analysis R package "Seurat" was employed to analyze the GC scRNA-seq data. The scRNA-seq data was normalized using the "LogNormalize" method and integrated using the "IntegrateData" function. The top 15 principal components were further dimensionally reduced using the Uniform Manifold Approximation and Projection (UMAP) technique. The cells were then clustered using the "FindClusters" function and annotated with typical cell markers. Subsequently, the macrophage group was subset for secondary clustering (dim=10, resolution=0.3) and the M1 or M2 subtype was identified for further analysis. Gene set variation analysis (GSVA) was then performed to evaluate the enrichment of hallmark gene sets in the difference gene list. The hallmark gene sets were acquired from the Molecular Signatures Database using the R package "msigdbr" with the specifications: species = "Homo sapiens" and category = "H".

Cell–cell communication and cell trajectory analysis (pseudotime analysis)

To study the interactions between various cell types, the "CellChat" function was used to infer the cell–cell interaction network information. We analyzed the number and weights/strength of intercellular communication and calculated the contribution of ligand–receptor pairs (L–R pairs) in different pathways. According to the changes in gene expression levels of different cell subsets over time, pseudotime analysis can be used to infer the cell differentiation track or the evolution process of cell subtypes during development. In our study, we used the "monocle" R package to conduct pseudotime analysis. By analyzing the developmental trajectories of macrophages, we were able to generate a density plot to visually represent the result.

Evaluation of the efficacy of immunotherapy

ICBatlas (http://bioinfo.life.hust.edu.cn/ICBatlas/) is a transcriptome-level data resource that comprehensively describes immune checkpoint blockade (ICB) treatment. The database integrates 25 gene expression profiling data sets from The Cancer Genome Atlas (TCGA), ArrayExpress, Gene Expression Omnibus (NCBI GEO) and other databases, including nine cancer types and 1515 ICB-treated patient samples. SPI1 expression levels in patients with GC who responded to ICB treatment and those who did not were evaluated. Another widely used database for evaluating the efficacy of immunotherapy is the Tumor Immunotherapy Gene Expression Resource (TIGER) database (http://tiger.canceromics.org/), which encompasses a wealth of data from tumor samples related to immunotherapy. The TIGER database was used to predict the responsiveness of immunotherapy with different SPI1$^+$CD68$^+$ TAMs infiltration levels.

Immune cell infiltration assessment

The CIBERSORT algorithm (https://cibersort.stanford.edu/) was used for evaluating immune cell infiltration in TCGA-GC patients, aiming to explore its association with SPI1$^+$CD68$^+$ TAMs. A comparative analysis of immune cell infiltration disparities was conducted via the Wilcoxon test, examining the contrast between high and low infiltration level of SPI1$^+$CD68$^+$ TAMs. Subsequently, the same statistical approach facilitated the quantification of infiltration variations in selected functional immune cell subsets.

Drug sensitivity analysis

To further understand the sensitivity of patients with GC to antiangiogenic agents, we also performed a drug sensitivity analysis for patients with different levels of SPI1$^+$CD68$^+$ TAMs infiltration using the R package "pRRophetic". By calculating the expression of SPI1 and CD68 in the TCGA-GC cohort, patients were divided into two groups with different levels of SPI1$^+$CD68$^+$ TAMs infiltration, and the IC50 of antineoplastic drugs was statistically analyzed by referring to the effect of more than 700 cell lines on 138 drugs in the Cancer Genome Project database (https://www.sanger.ac.uk/). We then performed statistical analysis to examine the differences in IC50 of antiangiogenic agents between the SPI1$^+$CD68$^+$ TAMs infiltration high and low groups.

Dual staining immunohistochemistry

To evaluate the infiltration of SPI1$^+$CD68$^+$ TAMs in patients with GC, we performed dual staining immunohistochemistry (DSIHC) on histopathologic slides. The slides were first dewaxed in an oven at 65°C for 2 hours and treated with xylene and gradient-reducing alcohol. Antigen retrieval was achieved by heating the slides in an Ethylene Diamine Tetraacetic Acid (EDTA) antigen repair solution (pH=6) for 15 min. To block any non-specific antigen-binding sites, goat serum blocking solution was applied to the slides for 30 min at 37°C. Subsequently, a mixture of anti-SPI1 antibody (mouse, Proteintech, 66618–2-Ig, diluted 1:250) and anti-CD68 antibody (rabbit, Proteintech, 25747–1-AP, diluted 1:500) was incubated on the slides overnight at 4°C. The next day, a mixture of secondary antibodies labeled with horseradish peroxidase (HRP) for mouse species and alkaline phosphatase (AP) for rabbit species was applied to the washed slides for 1 hour. The HRP-labeled antibodies stained brown and the AP-labeled antibodies stained pink with the staining kit treatment (ZS, DS-0003–120). Finally, the nucleus was counterstained with hematoxylin to stain it blue before the slides were fixed. The number of SPI1$^+$CD68$^+$ TAMs infiltration in the IHC specimens was then assessed.

Assessment of the SPI1$^+$CD68$^+$ TAMs infiltration in IHC specimens

Following DSIHC, SPI1 and CD68 were stained pink and brown, while SPI1$^+$CD68$^+$ TAMs displayed pink staining in the cytomembrane and brown staining in the nucleus. All specimens were examined at a 200×magnification view, and two of the most representative fields were captured from each tumor area. Two pathologists, who were blinded to the patient's information, identified SPI1$^+$CD68$^+$ TAMs (pink and brown) and SPI1$^-$CD68$^+$ TAMs (only pink). The SPI1$^+$CD68$^+$ TAMs score was calculated as the proportion of SPI1$^+$CD68$^+$ TAMs to all macrophages (which includes both SPI1$^+$CD68$^+$ and SPI1$^-$CD68$^+$ macrophages). In case of disagreement, the images were reviewed, and a consensus was reached between the two observers. The final score for each sample was determined by calculating the average score of the two fields. We performed Kaplan-Meier survival analysis to compare the high and low-score groups of patients with GC, who were divided based on the median value of the SPI1$^+$CD68$^+$ TAMs score. Additionally, we conducted DSIHC on a tissue microarray comprizing 76 samples from 31 patients with GC, including 40 primary gastric carcinoma and 36 metastatic tissues. The SPI1$^+$CD68$^+$ TAMs scores were calculated using the same method, and we analyzed the differences between primary and metastatic tissues.

Multiplex fluorescence immunohistochemistry

To detect several markers expressed on TAMs, T cells, and tumor cells within the GC tissue, a fluorescent multi-label kit (PANOVUE, TSA-RM-82758) was used, strictly adhering to the manufacturer's recommended protocols. After dewaxed and rehydrated, the GC tissue slides underwent heating antigen repair and goat serum blocking as described previously. Then, the slides were incubated with anti-SPI1 antibody at 37°C for 3 hours, followed by incubation with HRP-labeled secondary antibodies for 30 min. Finally, stained with the PANO tyramide signal amplification (TSA) buffer for 10 min. Then, the process of primary antibody incubation, followed by secondary antibody incubation and PANO TSA staining, was repeated until all markers were successfully stained. The results of the amount and distance between different cell types were calculated by HALO software.

Flow cytometry

Freshly isolated GC tissues were cut into small pieces and digested with Collagenase IV (Sigma) and DNase I (Sigma) at 37°C on a shaking bed for 30 min to achieve complete tissue digestion. The obtained cells were lysed with lysis buffer and kept on ice for 15 min. After erythrocyte lysis, the cells were counted and divided into blank and experimental groups. The samples were then incubated with a human BD Fc blocker and stained with the LIVE/DEAD Cell Imaging Kit (Invitrogen) in the dark at room temperature for 30 min. A series of antibodies, including CD45, CD68, CD86, CD206, and SPI1, were co-incubated with the cells in the stain buffer for 30 min. The stained cells were washed and resuspended in the staining buffer before being separated in a CytoFLEX LX flow cytometer and analyzed using FlowJo software (V.10.9). Surface markers of macrophages were examined in the same way. The antibodies used in flow cytometry are listed in online supplemental table S2.

THP1 cells transfection

SPI1-RNAi lentivirus was purchased from Genechem; Shanghai Genechem. Full name: RNAi-Easy-lentivirus (for suspension cells only). The vector name was GV766 and the element sequence was pRRLSIN-cPPT-U6-shRNA-SV40-puromycin. The control number used was CON609 and the control insertion sequence was TTCTCCGAAC-GTGTCACGT. Similarly, the same transfection method was applied to transfect SPI1 overexpression plasmid (SPI1) and its control vector (Vector) into THP1 cells. Transfection efficiency was evaluated through quantitative Reverse Transcription Polymerase Chain Reaction (qRT-PCR) and western blot analysis after 24 hours of infection.

Induction of macrophages

After induction of THP1 cells with Phorbol Myristate Acetate (PMA) at a working concentration of 100 ng/mL, M0 macrophages were obtained 24 hours later. After replacing the fresh complete medium, 100 ng/mL Lipopolysaccharide (LPS) working solution and 20 ng/mL IFN-γ working solution were added to M0 cells. M1 macrophages were harvested after 24 hours of continued culture. The M2-type macrophages were harvested 24 hours later if the M0 cells were further cultured with 20 ng/mL IL-4 and 20 ng/mL IL-13.

T-cell killing assay

Peripheral blood was collected from the donors in a predetermined volume, and lymphocytes were harvested through density gradient centrifugation using the Human Lymphocyte Separation Medium (Dakewe). Human CD3 T cell isolation kit (BioLegend) was then used to enrich T cells. The enriched T cells were then inoculated into culture media supplemented with interleukin-2 (IL-2), and co-cultured with conditional medium collected from macrophages exhibiting varying levels of SPI1 expression. Subsequently, the T cells were co-cultured with Human Gastric Adenocarcinoma Cells (AGS cells) for 24 hours, and the killing effect of T cells on tumor cells was detected by the Calcein/Propidium Iodide (PI) cell activity and cytotoxicity assay kit (Beyotime).

Chromatin immunoprecipitation assays

THP1 cells in a 15 cm culture dish were cross-linked with 1% formaldehyde at room temperature for 10 min. Glycine was then added to halt the reaction for 5 min at room temperature. The cells were subsequently washed twice with cold PBS and subjected to digestion with micrococcal nuclease as per the manufacturer's instructions using the chromatin immunoprecipitation (ChIP) Kit (#9003S, CST, USA, Boston). After harvesting the chromatin sample and extracting a 1% input sample, the samples were divided equally and incubated with an anti-SPI1 antibody (ab302623, Abcam), Histone H3 antibody (#4620, CST, included in the kit) or immunoglobulin G (#2729, CST, included in the kit), all above were conjugated to ChIP-Grade Protein G Magnetic Beads (#9006, CST, included in the kit) at 4°C overnight. The bound chromatin was then eluted using the reagents provided in the kit and quantitative PCR (qPCR) was performed after purification. The primer sequences used are listed in online supplemental table S3.

Animal experiments

Male Balb/c nude mice (4–5 weeks old) were procured from TopBiotech (Shenzhen, China). All animal experiments conducted in this study received approval from the Institutional Animal Care and Use Committee at TopBiotech (TOPGM-IACUC-2023–0027). Lentivirus vectors containing SPI1, shSPI1, and their respective controls were stably transfected into M0 macrophages derived from THP1 cells. The transfected M0 macrophages, mixed with MKN45 cells, were used to establish the tumor xenotransplantation model by subcutaneous injection into the right side of the nude mice. Tumor volumes were assessed on the 5th, 10th, 15th, and 20th days post-injection. The mouse model for intraperitoneal metastases was induced

5 days after intraperitoneal injection of MKN45-luciferase cells mixed with M0 macrophages transfected with SPI1 and shSPI1 lentiviral vectors. Abdominal metastasis was recorded by a small animal imaging instrument. This study adhered to ethical regulations governing animal research.

To better elucidate the antitumor effects of combined antiangiogenic and immunotherapy, we conducted in vivo experiments using 4 to 5-week-old NOD/SCID mice. HGC-27 cells transfected with luciferase were mixed with Vector and SPI1-overexpression macrophages to construct the model of abdominal metastases. Following successful modeling, human T cells isolated in vitro were injected into the mice (1 week). Subsequently, the mice were treated with either antiangiogenic therapy (Anti-VEGF, 5 mg/kg, every 3 days for four doses), immunotherapy (anti-programmed cell death protein-1 (PD-1), 10 mg/kg, every 3 days for four doses), or combination therapy according to their assigned groups (Vector or SPI1). The therapeutic effects were evaluated using a small animal imaging instrument.

Statistical analysis

R software (V.4.2.1) and associated R packages were used for data analyses, such as the "limma" package for difference analysis and the "survminer" package for survival analysis. Wilcoxon test was carried out to compare the differences among distinct groups. The Spearman correlation method was used to calculate the correlation coefficient and Cox regression analysis was used to identify the independent prognostic factors. All statistical analyses were bilateral, and $p < 0.05$ was considered statistically significant.

RESULTS

SPI1 was specifically expressed in macrophages and associated with metastasis

To investigate the expression of SPI1 in GC tissues, we evaluated the expression level of SPI1 with the scRNA sequence data. After rigorous quality control filters and doublet removal, a total of 53,359 cells and 26,251 genes were identified and included in the subsequent analysis (online supplemental figure S1A–B). Then, unsupervised clustering analysis was performed and defined 20 clusters with similar expression patterns (online supplemental figure S1C). Nine main cell populations with the expression of canonical markers were identified including B cells, CD8^{+} T cells, dendritic cells, endothelial cells, epithelial cells, fibroblasts, macrophages, mast cells, monocytes (figure 1A). The expression level and proportion of cell-specific markers in each cell subpopulation were displayed in dot plots (online supplemental figure S1D).

Among these nine cell types, SPI1 was mainly expressed in macrophages (figure 1B). To further explore the role of SPI1 expression in macrophage, we compared the expression level of SPI1 in primary tumor and metastatic

lesions in scRNA-seq data. The results showed that the expression of SPI1 in macrophages was higher in metastatic lesions than in primary sites (figure 1C–D). To verify this result, we performed DSIHC to evaluate the infiltration of SPI1^{+}CD68^{+} TAMs in primary tumor and metastasis lesions (figure 1E). The results showed that the infiltration of SPI1^{+}CD68^{+} TAMs was higher in multiple metastases lesions (ovary, colon, liver, and mesentery) than in primary sites (figure 1F). Flow cytometry showed that a larger number of SPI1^{+}CD68^{+} TAMs were observed in metastatic lesions than those in primary tumors (figure 1G–H). Taken together, these results indicated that the infiltration of SPI1^{+}CD68^{+} TAMs was increased in metastasis lesions in GC.

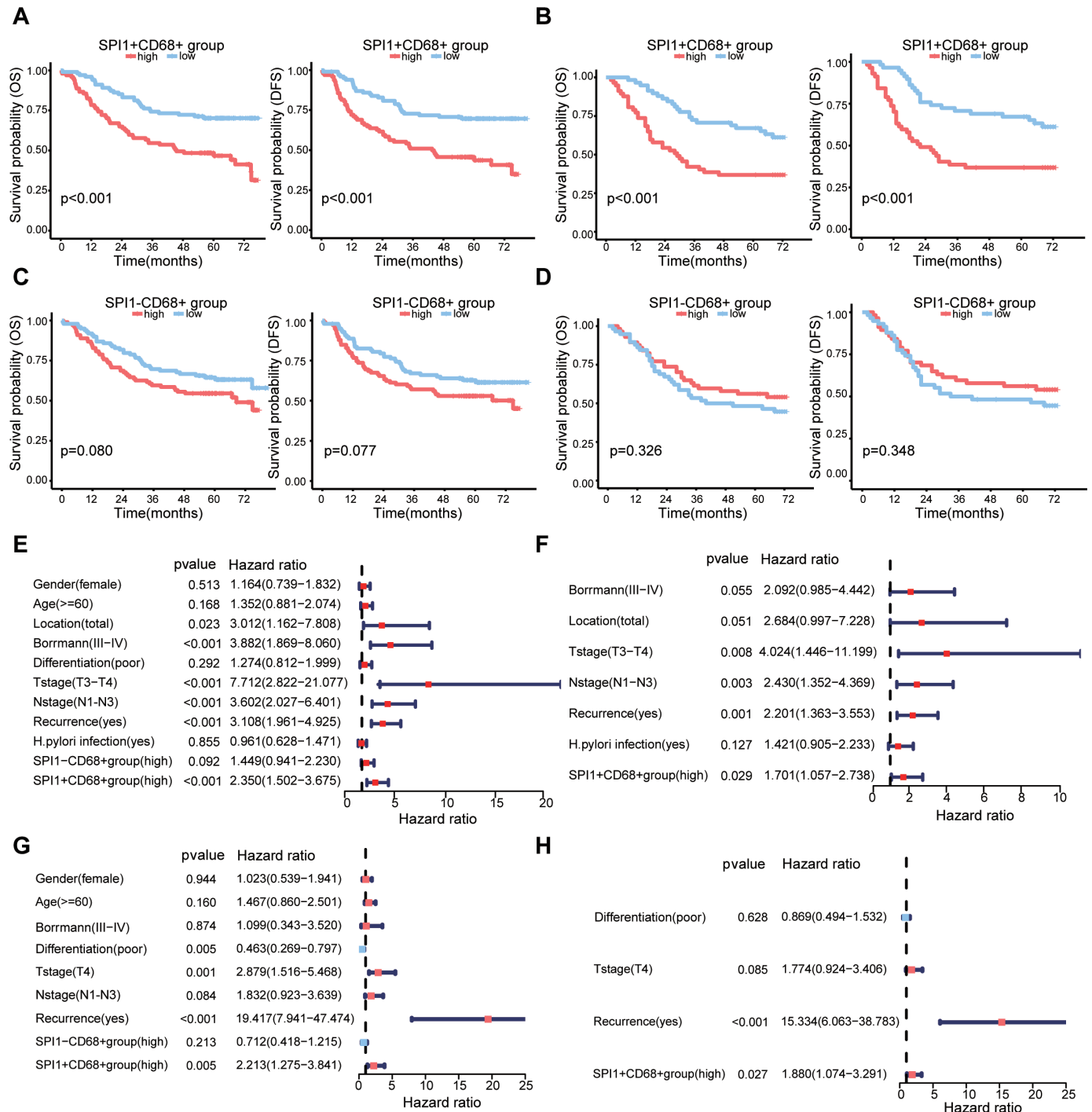#### SPI1 was an independent prognosis factor in GC

To investigate the prognosis significance of SPI1^{+}CD68^{+} TAMs in GC, we evaluated the infiltration of SPI1^{+}CD68^{+} TAMs in three independent cohorts. Patients were assigned into high and low groups according to the infiltration of SPI1^{+}CD68^{+} TAMs. Differences in clinicopathological characteristics between patients with high and low SPI1^{+}CD68^{+} TAMs levels were summarized in the online supplemental table S4. The survival analyses revealed that patients with more SPI1^{+}CD68^{+} TAMs infiltration had worse overall survival (OS) and disease-free survival (DFS) in the training (figure 2A) and external validation cohorts (figure 2B). However, the level of SPI1^{−}CD68^{+} TAMs infiltration did not predict an unfavorable prognosis in both cohorts (figure 2C–D). Additionally, in the TCGA-STAD cohort, we also observed the same results (online supplemental figures S2A–B). Furthermore, univariate and multivariate Cox regression analyses showed that SPI1^{+}CD68^{+} TAMs were an independent prognostic factor of patients with GC in the training cohorts (figure 2E–F, online supplemental table S5). This finding was corroborated in the external validation cohort and further substantiated by the TCGA-STAD cohort (figure 2G–H, online supplemental figure S2C–D).

SPI1 promoted M2-type macrophage polarization in GC

Macrophages could be polarized to M1 or M2-type macrophages in TME.[17] We further extracted macrophage and divided into M0, M1 (SOCS3, ITGAX, and IL1B) and M2 subtypes (CD163, CD204, and CD206) in scRNA-seq data (online supplemental figure S3A–B). Interestingly, we found that SPI1 was highly expressed in M2-type macrophages (online supplemental figure S3C). Additionally, pseudotime trajectory analysis was performed to determine the transition among specific cell type lineages and states. The trajectory analysis also yielded two different trajectory states (M1 and M2) (online supplemental figure S3D) and the evolution tree plot and density plot both revealed that SPI1 was mostly enriched at the end of M2-type macrophage (online supplemental figure S3E–F). Furthermore, flow cytometry showed that SPI1^{+}CD68^{+} TAMs were mainly concentrated in the M2-type macrophage group (figure 3A–B). Human
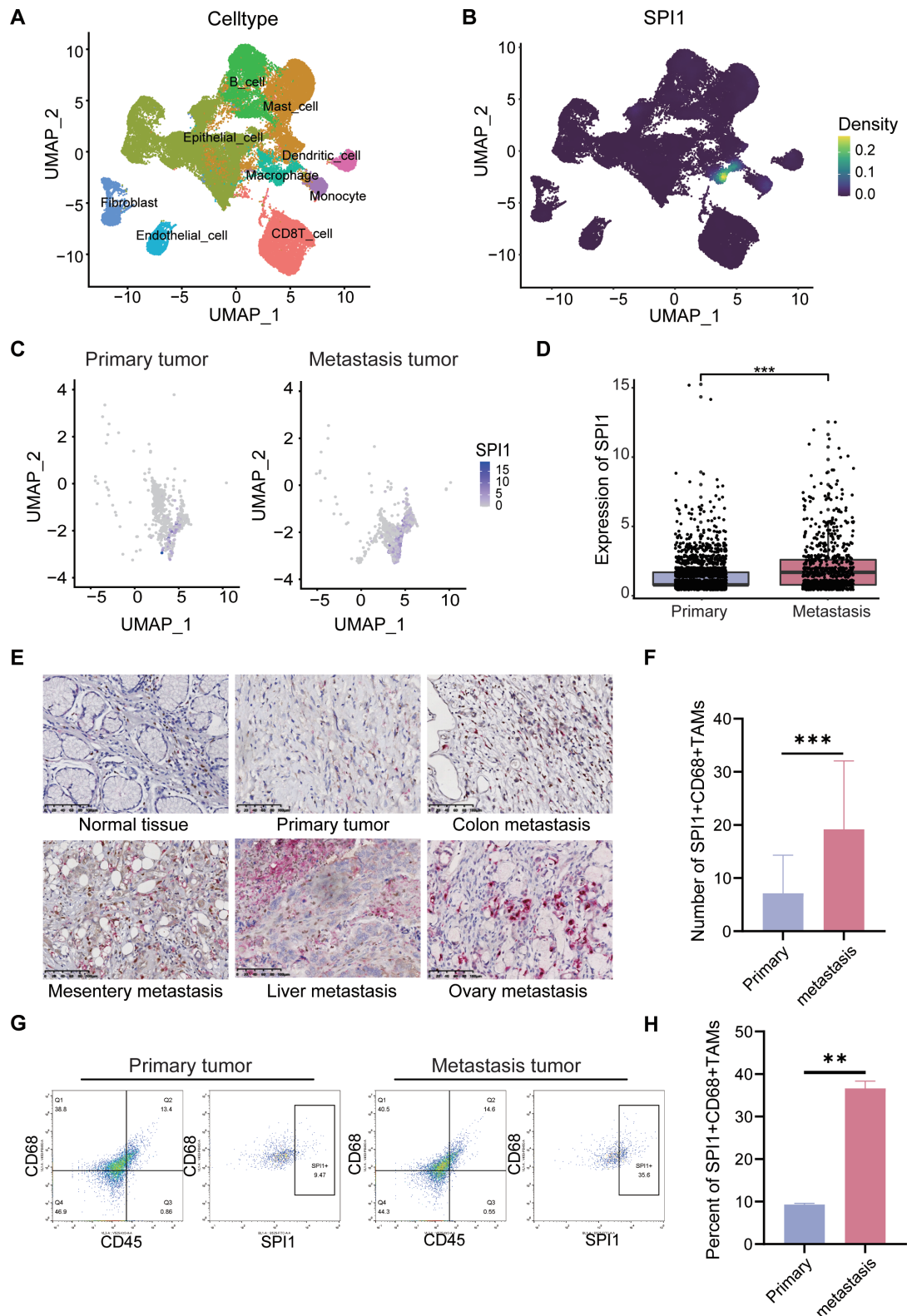
Figure 1 SPI1 was highly expressed in macrophages within the metastatic lesions of gastric cancer. (A) UMAP representation colored according to different cell types. (B) Density plot of SPI1 expression distribution in scRNA sequencing data. (C) UMAP indicated SPI1 staining of macrophages in primary and metastasis gastric cancer (GC). (D) Differential analysis of SPI1 expression in the primary and metastasis tumor of GC in scRNA sequencing data. (E) Infiltration of SPI1^{+}CD68^{+} TAMs in normal tissue, primary tumor, and metastasis sites of GC. (F) Differential analysis of SPI1^{+}CD68^{+} TAMs infiltration between primary and metastasis tumor according to double immunohistochemical staining. (G) SPI1^{+}CD68^{+} TAMs were screened by flow cytometry in primary and metastasis tumor of patients with GC. (H) Quantitative analysis of SPI1^{+}CD68^{+} TAMs infiltration based on flow cytometry. scRNA, single-cell RNA; SPI1, Spi-1 proto-oncogene; TAMs, tumor-associated macrophages; UMAP, Uniform Manifold Approximation and Projection.

Figure 2 SPI1+CD68+ TAMs was an independent prognostic factor in patients with metastatic gastric cancer. (A) Overall survival (OS) and disease-free survival (DFS) of patients with gastric cancer (GC) in different SPI1+CD68+ TAMs groups in the training cohort. (B) OS and DFS of patients with GC in different SPI1+CD68+ TAMs groups in the external validation cohort. (C) OS and DFS of patients with GC in different SPI1−CD68+ TAMs groups in the training cohort. (D) OS and DFS of patients with GC in different SPI1−CD68+ TAMs groups in the external validation cohort. (E) Univariate cox regression analysis of patients with GC in the training cohort. (F) SPI1+CD68+ TAMs was an independent prognostic factor of patients with GC in the training cohort. (G) Univariate cox regression analysis of patients with GC in the external validation cohort. (H) SPI1+CD68+ TAMs was an independent prognostic factor of patients with GC in the external validation cohort. SPI1, Spi-1 proto-oncogene; TAMs, tumor-associated macrophages.

THP-1 monocytes were differentiated into M1 and M2 subtypes of macrophages after induction. The expression of chemokines and cytokines were examined to characterize different macrophage subtype. The results

indicated that the messenger RNA (mRNA) level of SPI1 was higher in M2-type macrophages (figure 3C).

To further explore the mechanism of SPI1 in macrophages, we constructed cell lines with stable knockdown
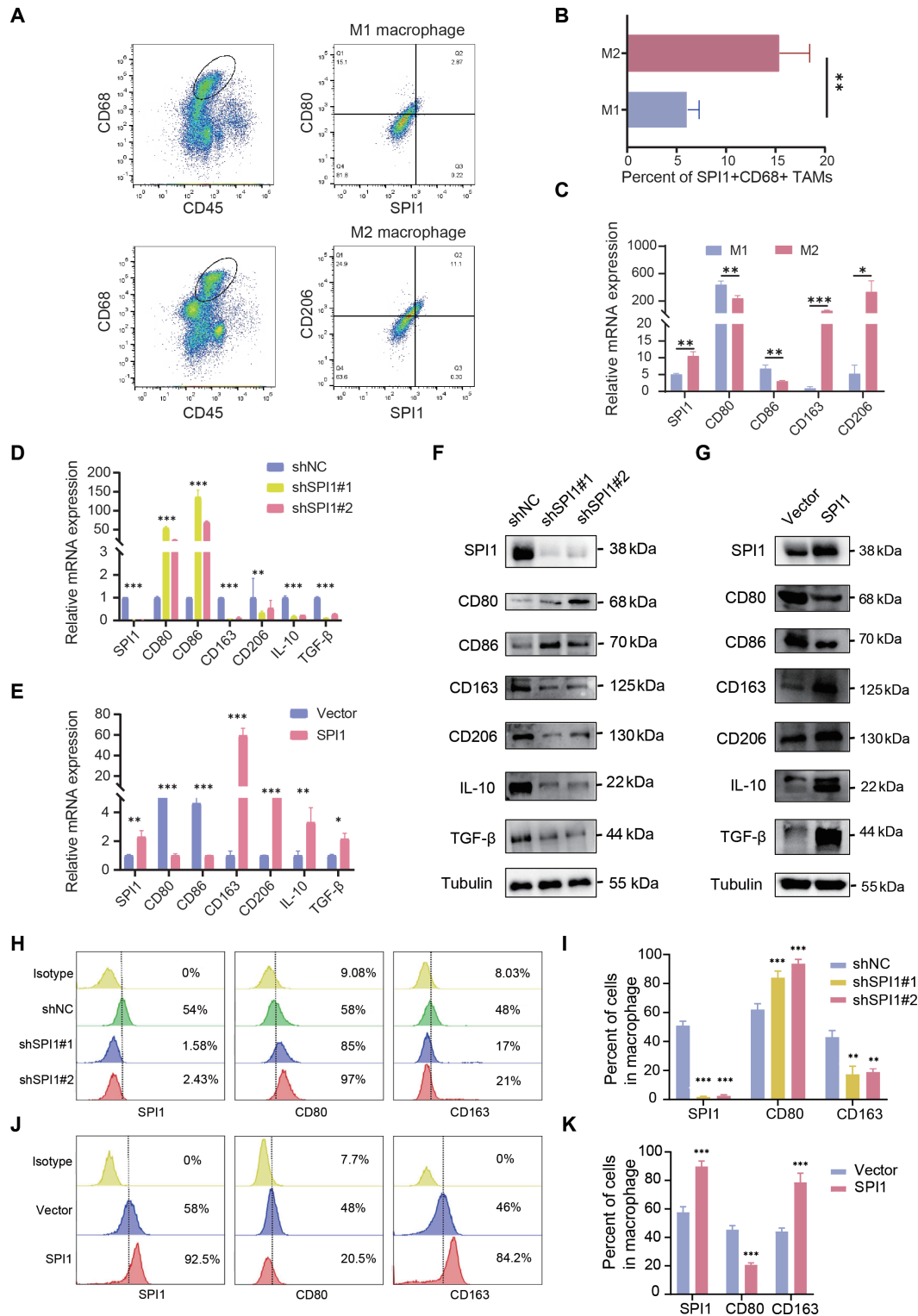
Figure 3 SPI1 was associated with M2 polarization of macrophages. (A) Screening M1/M2 macrophages used flow cytometry with CD45, CD68, CD80, CD206 and SPI1 in patients with gastric cancer (GC). (B) Quantitative analysis of SPI1+CD68+ TAMs infiltration in M1 and M2 type based on flow cytometry of patients with GC. (C) The markers of induced M1 and M2-type macrophages were detected by qRT-PCR. (D) Detecting the macrophage-related markers with qRT-PCR after SPI1 knockdown. (E) qRT-PCR was used to detect the macrophage-associated markers after SPI1 overexpression. (F) Western blot was used to detect the macrophage-related markers after SPI1 knockdown. (G) Macrophage-related markers were detected with western blot after SPI1 overexpression. (H) Flow cytometry was used to detect the macrophage-related markers after SPI1 knockdown. (I) Quantitative analysis of flow cytometry in SPI1 knockdown macrophages. (J) Flow cytometry was used to detect the macrophage-related markers after SPI1 overexpression. (K) Quantitative analysis of flow cytometry in SPI1 overexpression macrophages. IL-10, interleukin-10; mRNA, messenger RNA; qRT-PCR, quantitative Reverse Transcription Polymerase Chain Reaction; SPI1, Spi-1 proto-oncogene; TAMs, tumor-associated macrophages.

SPI1 in THP1 cells (shSPI1). The protein and mRNA level of M2 markers (CD163, CD206) were decreased in M0 macrophages (induced by THP1 cells) with SPI1 knockdown (figure 3D), while the expression of M1 markers (CD80, CD86) was increased (figure 3F). Furthermore, we also transfected THP1 cells with the control vector (Vector) and SPI1 overexpression lentivirus (SPI1). The changes in macrophage markers indicated that SPI1 overexpression promoted M2 polarization of macrophage (figure 3E and G). Flow cytometry analysis showed that CD80 was increased and CD163 was decreased in macrophages with SPI1 knockdown (figure 3H–I), while the opposite trend was observed in macrophages with SPI1 overexpressed (figure 3J–K). These results indicated that SPI1 promoted M2-type macrophage polarization.

SPI1$^+$CD68$^+$ TAMs were associated with VEGF pathway

To explore the mechanism of the SPI1$^+$CD68$^+$ TAMs in GC metastasis, we performed pathway enrichment analysis between SPI1^{High} TAMs and SPI1^{Low} TAMs using GSVA analysis in scRNA-seq data. The results showed that SPI1^{High} TAMs were enriched in the inflammatory response, epithelial-mesenchymal transition, and angiogenesis (figure 4A). Additionally, we performed cell–cell communication analysis to investigate the interaction between TAMs and other cells. We found that TAMs were closely interacted with endothelial cells (online supplemental figure S4A–B). Furthermore, we identified that SPI1^{High} TAMs interacted more strongly with endothelial cells than SPI1^{Low} TAMs (figure 4B). The VEGF pathway is one of the most critical pathways that associated with angiogenesis in tumor.[18] In the VEGF pathway, SPI1^{High} TAMs exhibited a stronger association with endothelial cells than SPI1^{Low} TAMs (figure 4C). Moreover, the L–R pair VEGFA-VEGFR1/VEGFR2 had the highest contribution (online supplemental figure S4C). In the external validation cohort, we found that patients with higher SPI1$^+$CD68$^+$ TAMs infiltration level were more sensitive to bevacizumab, an antiangiogenic drug that is widely used in clinical practice. Conversely, no statistically significant difference in treatment response was observed within the SPI1$^-$CD68$^+$ TAMs group (figure 4D). Multiplex fluorescence immunohistochemistry was used to assess the spatial distribution of SPI1$^+$CD68$^+$ TAMs and vessels (figure 4E). We found that the infiltrating number of SPI1$^+$CD68$^+$ TAMs around the perivascular area was significantly higher than that of SPI1$^-$CD68$^+$ TAMs (figure 4F). Furthermore, the spatial distance between vessels and SPI1$^+$CD68$^+$ TAMs was closer than that of SPI1$^-$CD68$^+$ TAMs (figure 4G). These results indicated that SPI1 was closely related to tumor angiogenesis in spatial.

The drug-sensitivity analysis revealed that patients with high SPI1$^+$CD68$^+$ TAMs infiltration had lower IC50 for antiangiogenic agents compared with patients with low SPI1$^+$CD68$^+$ TAMs infiltration (online supplemental figure S4D–G). These results indicated that patients with high SPI1$^+$CD68$^+$ TAMs infiltration may be more sensitive and responsive to the antiangiogenic agents. Therefore,

we hypothesized that SPI1$^+$CD68$^+$ TAMs may play a critical role in angiogenesis.

SPI1 facilitated GC cell growth and metastasis in vivo

To validate the function of SPI1 in vivo, we constructed THP1 cells with stable knockdown or overexpressed SPI1, which were induced into macrophages. After mixed with transfected macrophages, MKN45 cells were subcutaneously injected into the mouse to establish a xenograft tumor model (figure 5A). The results showed that SPI1 overexpression significantly increased both the volume and weight of the tumors, while these effects were reduced when SPI1 was knocked down (figure 5B–C). To further investigate the impact of SPI1 on metastasis in vivo, we injected transfected macrophages and MKN45-luciferase cells into the peritoneal cavity of mice. Based on bioluminescence intensity measured in the IVIS system, SPI1 overexpression increased the number of metastatic nodules in the abdominal cavity, whereas SPI1 knockdown significantly reduced (figure 5D). The trend in fluorescence intensity alterations was also positively correlated with the expression levels of SPI1 (figure 5F). We concurrently enumerated the number of metastatic nodules present in the peritoneal cavity (figure 5E). The quantity of metastatic nodules within the peritoneal cavity was found to correlate with the expression levels of SPI1 (figure 5G). The survival curves showed that SPI1 was associated with a shorter survival time (figure 5H). These findings illuminated that SPI1 could promote tumor growth and metastasis in vivo.

SPI1 modulated the migratory and tube formation of endothelial cells

Wound scratch assay showed that the migration of endothelial cell was decreased after co-culturing with a conditioned medium of M0 macrophage with SPI1 knockdown (figure 6A). Meanwhile, overexpression of SPI1 in macrophages promoted the migration of endothelial cell (figure 6B). Tube formation assay revealed a diminished capacity for angiogenesis on SPI1 knockdown (figure 6C). In contrast, elevated SPI1 expression was found to augment the angiogenic potential of endothelial cells (figure 6D). We performed immunohistochemistry to assess the expression level of SPI1, CD31, and VEGFA in the same patient (online supplemental figure S5A), which demonstrated that the expression of SPI1 was positively correlated with CD31 and VEGFA (online supplemental figure S5B–C). To better observe the relationship between SPI1 and tumor neovascularization, we performed H-E staining on sections of subcutaneously transplanted tumors in mice (online supplemental figure S5D). The results revealed that SPI1 overexpression notably increased the number of tumor neovascularization compared with SPI1 knockdown (online supplemental figure S5E). Taken together, these findings suggested that SPI1 could promote angiogenesis in GC.

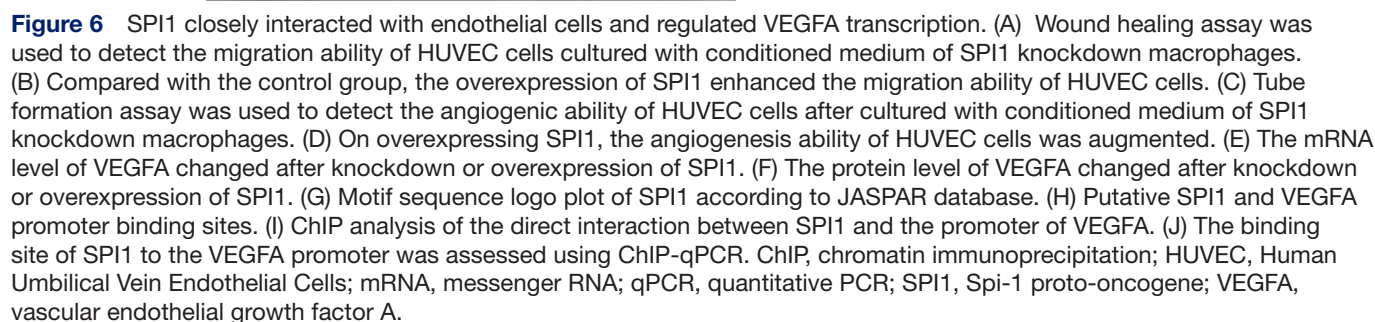Based on the aforementioned results, we further explored the regulatory role of SPI1 in angiogenesis. We
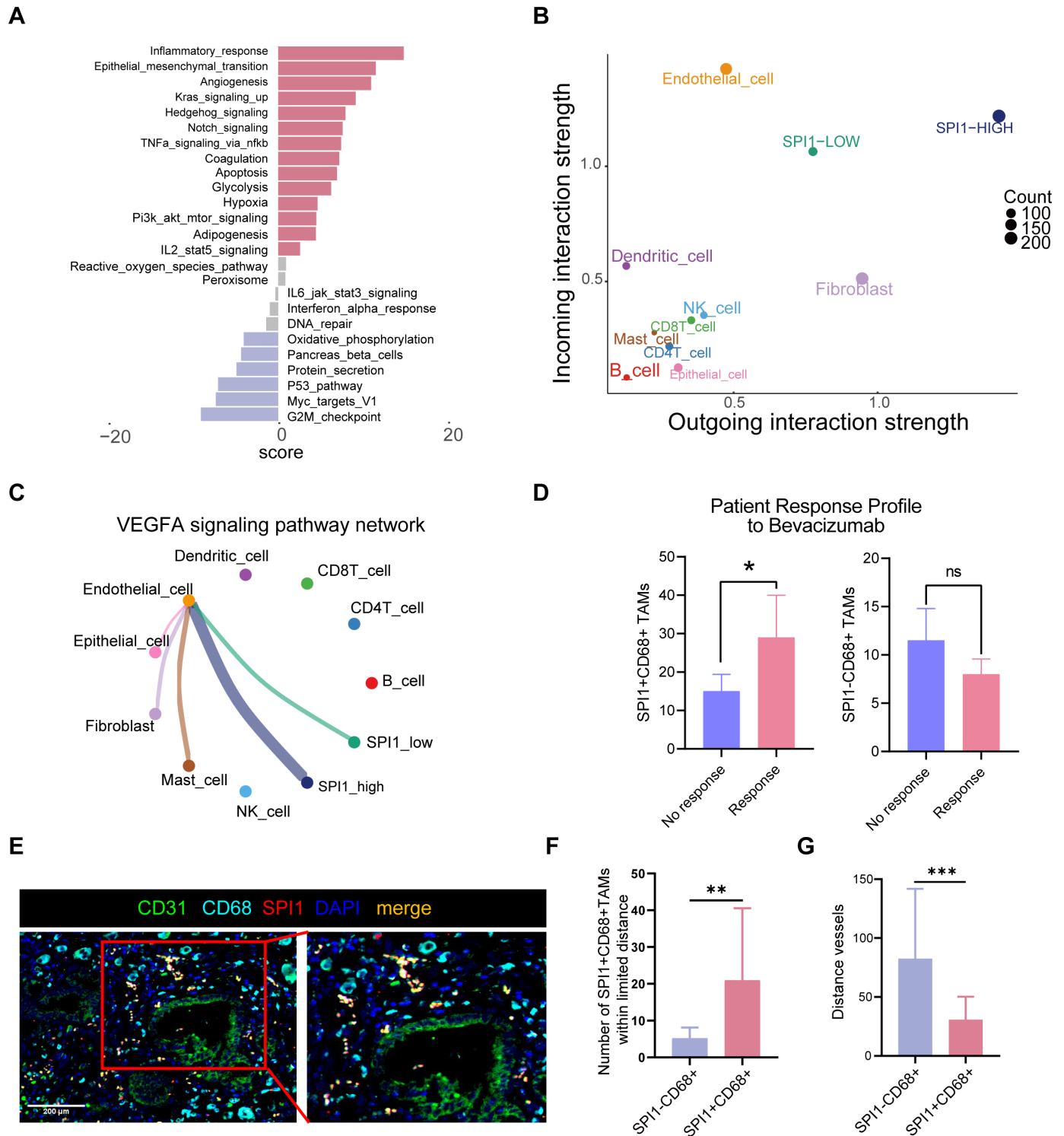
Figure 4 SPI1⁺CD68⁺ TAMs promoted tumor angiogenesis through VEGF pathway. (A) GSVA analysis between SPI1-high and SPI1-low TAMs groups in scRNA sequencing data. (B) Incoming and outgoing interaction strength in different types of cells. (C) Cell–cell communication between different cell types in the VEGF signaling pathway. (D) Response to bevacizumab in patients with different TAMs infiltrates in the external validation cohort. (E) Immunofluorescence revealed the infiltration of SPI1⁺CD68⁺ TAMs around the tumor blood vessels (CD31 marked). (F) Difference in the number of SPI1⁺CD68⁺ TAMs and SPI1⁻CD68⁺ TAMs around tumor vessels. (G) Difference in distance between blood vessels with SPI1⁺CD68⁺ TAMs and SPI1⁻CD68⁺ TAMs. DAPI, 4',6-Diamidino-2-Phenylindole; GSVA, gene set variation analysis; NK, Natural Killer cells; scRNA, single-cell RNA; SPI1, Spi-1 proto-oncogene; TAMs, tumor-associated macrophages; VEGFA, vascular endothelial growth factor A.
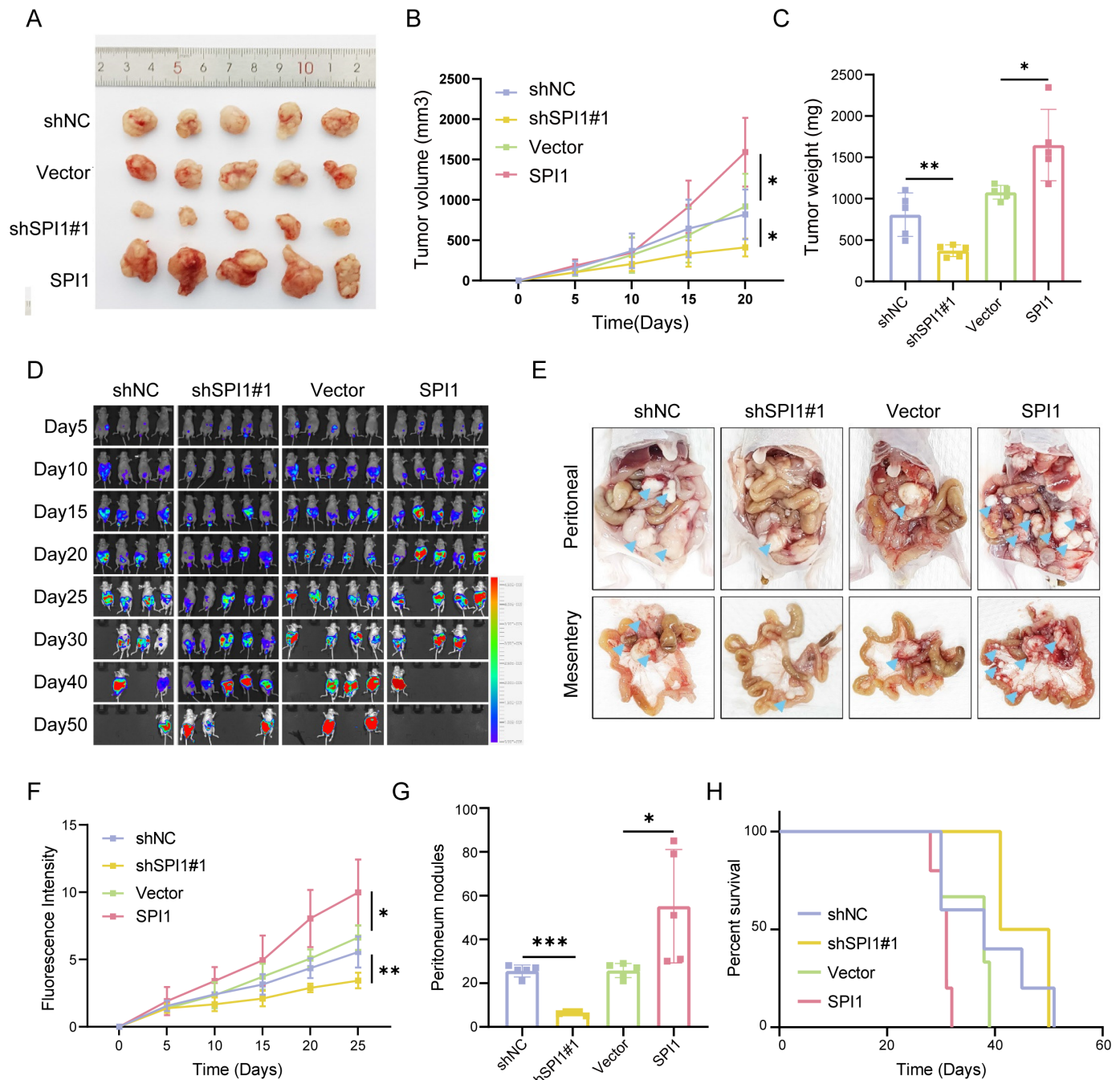
Figure 5 The role of SPI1 in GC cell growth and metastasis in vivo. (A) The representative images of the xenograft tumor. (B) Quantitative analysis of tumor growth curve. (C) Quantitative analysis of tumor weight in different SPI1 expression group. (D) Bioluminescence images of tumor-bearing mice individually treated with shNC, shSPI1, Vector, SPI1 transfected macrophages at day 5, 10, 15, 20, 25, 30, 40, and 50. (E) Representative photographs of peritoneum and mesentery metastasis lesions in different SPI1 expression groups. (F) The fluorescence intensity of tumors in various groups of mice. (G) Quantitative analysis of peritoneum nodules. (H) Survival curves of mice in different groups. GC, gastric cancer; SPI1, Spi-1 proto-oncogene.

found that the protein and RNA expression of VEGFA was decreased after SPI1 knockdown and increased after SPI1 was overexpressed (figure 6E–F). Additionally, ELISA demonstrated that the secretion of VEGFA was elevated after SPI1 overexpression (online supplemental figure S5F). Tracing the origin of VEGFA, we used scRNA-seq data and found that macrophages were the major source of VEGFA in patients with GC (online supplemental figure S6A). Additionally, VEGFA and SPI1

were co-expressed in macrophages (online supplemental figure S6B). Then we leveraged single-cell sequencing data to analyze M2-type macrophages, revealing that cluster 0 exhibited a higher SPI1 expression level among the three M2-type macrophage subsets (online supplemental figure S6C–D). Further, the AddModuleScore function was used to evaluate the M2-type macrophage subpopulations, indicating that cluster 0 possessed a higher angiogenesis score (online supplemental figure

Figure 6 SPI1 closely interacted with endothelial cells and regulated VEGFA transcription. (A) Wound healing assay was used to detect the migration ability of HUVEC cells cultured with conditioned medium of SPI1 knockdown macrophages. (B) Compared with the control group, the overexpression of SPI1 enhanced the migration ability of HUVEC cells. (C) Tube formation assay was used to detect the angiogenic ability of HUVEC cells after cultured with conditioned medium of SPI1 knockdown macrophages. (D) On overexpressing SPI1, the angiogenesis ability of HUVEC cells was augmented. (E) The mRNA level of VEGFA changed after knockdown or overexpression of SPI1. (F) The protein level of VEGFA changed after knockdown or overexpression of SPI1. (G) Motif sequence logo plot of SPI1 according to JASPAR database. (H) Putative SPI1 and VEGFA promoter binding sites. (I) ChIP analysis of the direct interaction between SPI1 and the promoter of VEGFA. (J) The binding site of SPI1 to the VEGFA promoter was assessed using ChIP-qPCR. ChIP, chromatin immunoprecipitation; HUVEC, Human Umbilical Vein Endothelial Cells; mRNA, messenger RNA; qPCR, quantitative PCR; SPI1, Spi-1 proto-oncogene; VEGFA, vascular endothelial growth factor A.

S6E–F). The results indicated that SPI1$^+$CD68$^+$ TAMs, as a subgroup of angiogenic M2-type macrophages, were the main source of VEGFA secretion.

Considering SPI1's role as a transcription factor, we questioned whether it regulates VEGFA transcription. Subsequently, motif sequences of SPI1 were identified in the JASPAR database (http://jaspar.genereg.net) (figure 6G). The results identified three predicted SPI1 binding sites in the VEGFA promoter region (figure 6H). The ChIP assays were verified using agarose gel electrophoresis (figure 6I). Subsequent ChIP-qPCR analyses also demonstrated that SPI1 could bind to the promoter of VEGFA (figure 6J). Collectively, these findings demonstrated that SPI1 could induce the expression of VEGFA in macrophages by activating the transcriptional activity via binding to the promoter region.

SPI1$^+$CD68$^+$ TAMs may promote an immunosuppressive microenvironment in GC

Macrophage, especially the M2-type macrophage, is one of the central drivers of the immunosuppressive TME, and could regulate the function of T cell. PD-1$^+$CD8$^+$ T cells have been associated with immunosuppressive microenvironment in various malignancies. Previous studies have shown that immunotherapy combined with antiangiogenic therapy could significantly improve the survival of patients with metastatic GC. These results demonstrated that the combination of immunotherapy and antiangiogenic treatment could become a promising strategy in antitumor therapy. In light of these considerations, we further explored the role of SPI1 in the immune microenvironment. The responsiveness of patients with GC to immunotherapy was analyzed using the ICBaltas data set. Patients with high SPI1 expression were found to respond better to PD-1 immune checkpoint therapy compared with those with low SPI1 expression (online supplemental figure S7A). TIGER database contains a large amount of data related to tumor immunotherapy, especially involving transcriptomics data. After conducting differential expression analysis on the matrix normalized by CD68, the results indicated that patients with high SPI1 expression exhibited significantly greater responsiveness to PD-1 immunotherapy in project PRJEB25780 (online supplemental figure S7B). Moreover, the TIGER database was employed to forecast the immunotherapeutic responsiveness of SPI1, revealing an AUC (area under the curve) of 0.6985 for SPI1, which surpassed most of the established predictors for immunotherapy effectiveness (online supplemental figure S7C). This outcome underscores SPI1's notable proficiency in forecasting immunotherapy responses, thereby emphasizing its robust predictive capacity. Using the CIBERSORT database to investigate variances in immune cell infiltration among TCGA-STAD patients categorized into different SPI1$^+$CD68$^+$ TAMs groups, the findings reveal that patients with more SPI1$^+$CD68$^+$ TAMs infiltration have a heightened extent of immune cell infiltration such as M2-type macrophages and regulatory T cells (Treg) (online supplemental figure

S7D–E). The results of immune checkpoint score analysis based on the TCGA-STAD cohort showed that patients with higher level of SPI1$^+$CD68$^+$ TAMs infiltration tend to have a more favorable therapeutic effect (online supplemental figure S7F). Furthermore, we explored the relationship between TAMs and CD8$^+$ T cells using cell–cell communication analysis in scRNA-seq data. The results also showed that SPI1^{high} TAMs are more closely interacted with CD8$^+$ T cells (online supplemental figure S7G). Higher expression levels of PD-1 and other immunosuppression markers were observed in the SPI1$^+$CD68$^+$ TAMs high group than those in the SPI1$^+$CD68$^+$ TAMs low group (online supplemental figure S7H). We also conducted a correlation analysis between SPI1 and several immunosuppressive markers, including PDCD1 (PD-1), CTLA4, LAG3, PRDM1, and HAVCR2 in the TCGA-STAD cohort. The results showed that the expression of SPI1 was positively correlated with these immunosuppressive markers (online supplemental figure S7I). To validate these findings in GC tissues, we conducted multiplex immunofluorescence to evaluate the infiltration levels of SPI1$^+$ and PD-1$^+$ cells, which showed PD-1$^+$ cells were more infiltrated in patients with high SPI1 expression compared with those with low SPI1 expression (online supplemental figure S8A–B). To investigate the interplay between macrophages and T cells, we also undertook cell killing assay based on T cell co-culture with different SPI1 expression macrophage (online supplemental figure S8C). The findings demonstrated that the cytotoxic activity of T cells was notably suppressed following their co-culture with macrophages that overexpressed SPI1 (online supplemental figure S8D). Taken together, these data suggested that SPI1$^+$CD68$^+$ TAMs may be associated with the exhaustion of CD8$^+$ T cells in immunosuppressive TME.

In vivo response to anti-PD-1 immunotherapy and antiangiogenic treatment

To further validate the treatment effect of combining antiangiogenic and immunotherapy, we collected imaging data and Combined Positive Score (CPS) from patients undergoing immunotherapy at our clinical research center. Subsequently, we analyzed the treatment responses and the expression of programmed death-ligand 1 (PD-L1), SPI1, and CD68 (figure 7A). The results suggested that patients with more SPI1$^+$CD68$^+$ TAMs infiltration were more sensitive to immunotherapy (figure 7B), and SPI1 and PD-L1 expression were positively correlated (figure 7C). To assess the predictive value of SPI1 compared with the CPS score, we constructed a receiver operating characteristic curve (figure 7D–G). The AUC values for each group were 0.757 (CPS score), 0.560 (CD68$^+$ cells), 0.706 (SPI1$^+$CD68$^+$TAMs), and 0.816 (combined CPS score with SPI1$^+$CD68$^+$TAMs). The analysis revealed that the SPI1$^+$CD68$^+$TAMs showed good prediction performance (AUC: 0.757), and the combined treatment group had better prediction performance than the CPS score or SPI1$^+$CD68$^+$TAMs alone.
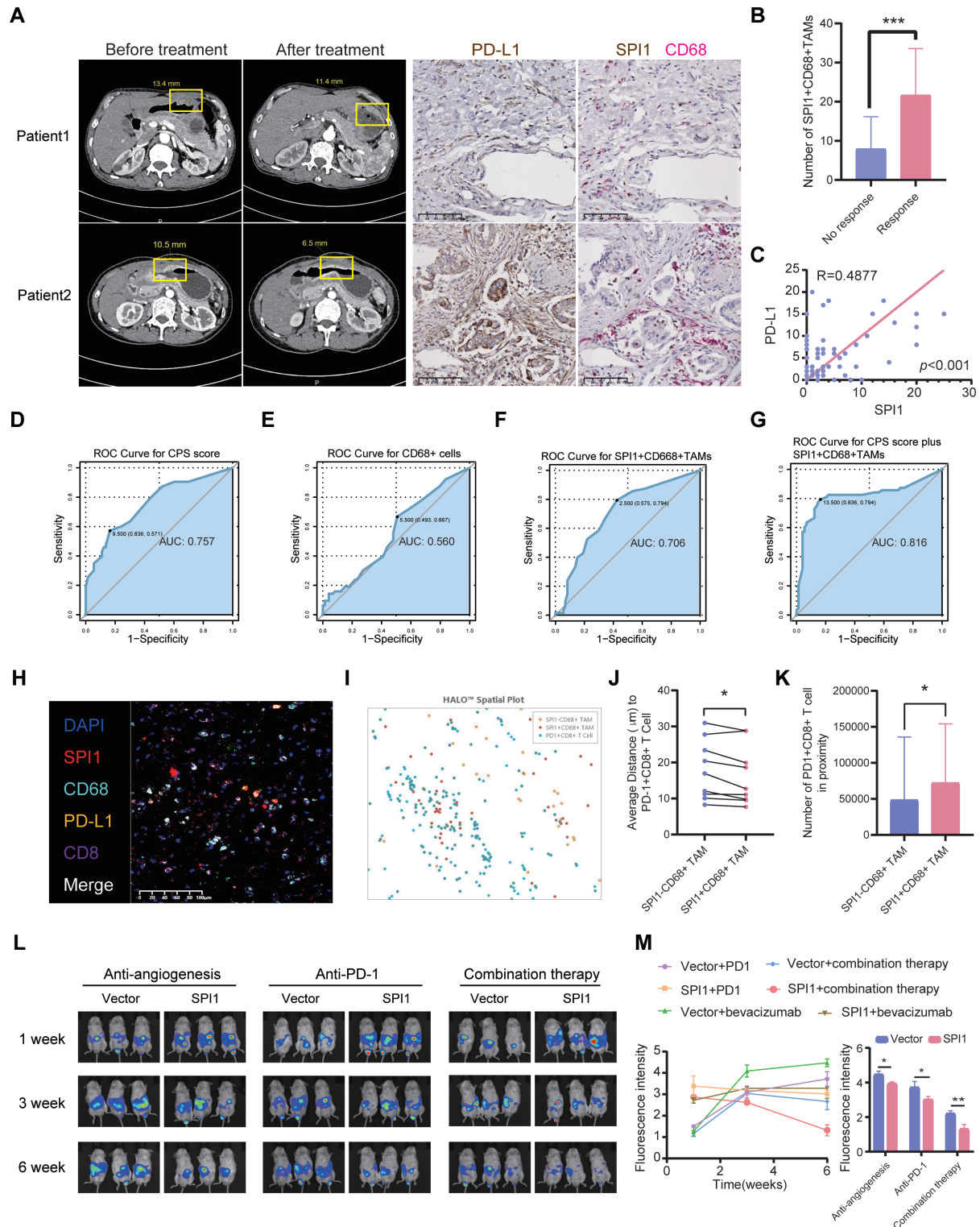
Figure 7 In vivo response to anti-PD-1 immunotherapy and antiangiogenesis treatment. (A) Response to immunotherapy in patients with different CPS scores and SPI1+CD68+ TAMs infiltration. (B) Difference analysis of immunotherapy response in patients with different SPI1+CD68+ TAMs infiltration. (C) Correlation analysis of SPI1 and PD-L1. (D–G) ROC curve of CPS score, CD68+ cells, SPI1+CD68+ TAMs, and CPS score plus SPI1+CD68+ TAMs. (H) Multiple immunofluorescences staining of PD-1+CD8+ T cells and SPI1+CD68+ TAMs. (I) Spatial distribution of SPI1+CD68+ TAMs, SPI1−CD68+ TAMs and PD-1+CD8+ T cells analyzed by HALO. (J) Average distance from PD-1+CD8+ T cells to SPI1+CD68+ TAMs and SPI1−CD68+ TAMs (p<0.05). (K) The discrepancy in the quantity of SPI1+CD68+ TAMs and SPI1−CD68+ TAMs surrounding PD-1+CD8+ T cells (p<0.05). (L) Bioluminescence images of NOD/SCID mice with different treatment in week 1, 3, and 6. (M) The fluorescence intensity of intraperitoneal tumors in various groups of mice. CPS, Combined Positive Score; DAPI, 4',6-Diamidino-2-Phenylindole; PD-1, programmed cell death protein-1; PD-L1, programmed death-ligand 1; ROC, receiver operating characteristic; SPI1, Spi-1 proto-oncogene; TAMs, tumor-associated macrophages.

These results suggested that the infiltration of SPI1+CD68+TAMs possessed good predictive performance in evaluating the response of immunotherapy. Subsequently, we employed multiplex immunofluorescence staining to label SPI1+CD68+ TAMs and PD-1+CD8+ T cells (figure 7H), and spatial plots were performed using HALO software (figure 7I). On analyzing the spatial distances between distinct cell types, we observed that PD-1+CD8+ T cells were in closer spatial proximity to SPI1+CD68+ TAMs rather than SPI1−CD68+ TAMs (figure 7J). Moreover, more PD-1+CD8+ T cells were in close proximity to SPI1+CD68+ TAMs than to SPI1−CD68+ TAMs (figure 7K). Finally, in vivo experiments in NOD/SCID mice showed that the degree of SPI1+CD68+ TAMs infiltration was closely related to the efficacy of immunotherapy, especially after being combined with antiangiogenic therapy (figure 7L). These results indicated the therapeutic potential and prediction value of SPI1+CD68+ TAMs in combination treatment (figure 7M).

DISCUSSION

TAMs are among the most important cells in TME, capable of fostering immunosuppression and enabling the immunological escape of tumor cells through the production of cytokines, chemokines, and growth factors.[19] TAMs play an essential role in this process by promoting tumor cell metastasis and providing a facilitating microenvironment for cancer.[20] TAMs have traditionally been categorized into M1 and M2-type subtypes. M1 is commonly known as the antitumor subtype, whereas M2 is considered to promote tumor growth.[21] However, ongoing research has unveiled an ever-expanding diversity of TAMs subtypes with varying functions.[19 22 23] Within our scRNA sequencing data, more than two distinct clusters were also discerned in the macrophage subgroup. This discovery underscores the limitations of the traditional binary classification approach, as it fails to meet the demands of research. Metastasis is a common malignant characteristic observed in tumors and a leading cause of death in GC.[24] This process often involves mechanisms such as drug resistance and immune suppression, presenting an unresolved challenge for researchers.[25] Therefore, excavating TAMs subpopulations associated with metastasis is incredibly beneficial in developing a responsive therapeutic strategy in patients with GC.

The results of IHC showed that CD68 has been employed as a valuable cell marker for identifying monocytes/macrophages. CD68 paired with other TAMs cellular markers, has been proven to be a good prognostic predictor of survival for patients with cancer.[26] SPI1, a key factor regulating myeloid differentiation, is intrinsically related to macrophage maturation and polarization.[27 28] However, few studies have reported the role of SPI1 in solid tumors. In the present study, we analyzed the infiltration of SPI1+CD68+ TAMs in the primary and metastatic tissues of patients with GC and found that more infiltration of SPI1+CD68+ TAMs was correlated with poor

survival. However, there was no significant correlation between SPI1−CD68+ TAMs and OS/DFS. These results indicated that SPI1 could further enhance the predictive ability of CD68. Most importantly, SPI1+CD68+ TAMs were abundantly infiltrated in metastatic tissues, which also demonstrated the prediction ability in tumor metastasis. What is more, previous studies demonstrated that M2-type macrophages are involved in angiogenesis, immune regulation, tumor formation, and progression.[29 30] Qian et al found that SPI1 plays a critical role in macrophage polarization and asthmatic inflammation.[31] Liu et al identified ATP6V0D2 as an induced feedback inhibitor of asthma disease severity by promoting SPI1 lysosomal degradation, which may result in reduced macrophage polarization.[15] Therefore, THP1 cells were used to verify the effect of SPI1 on macrophage polarization in vitro. More SPI1+CD68+ TAMs were found to be infiltrated in M2-type macrophages in our study, which suggested that SPI1 may be involved in GC metastasis via affecting macrophage polarization.

Angiogenesis is an essential component of the tumor metastatic process.[32] Both proangiogenic and antiangiogenic factors regulate angiogenesis modulation. Tumor-driven hypoxia increases the expression of proangiogenic factors, leading to the formation of new blood vessels, which are essential for tumor survival and proliferation.[33] Furthermore, tumor recurrence and metastasis are often accompanied by the formation of abnormal blood vessels.[34] The abnormal structure and function of these vessels contribute to the deterioration of the tumor by impairing blood perfusion, which creates a hypoxia and acidic, immunosuppressive microenvironment.[35] Additionally, the leaky nature of these abnormal vessels could facilitate the entry of shed cancer cells into the bloodstream.[32] Thus, tumor cells could disseminate to distant organs and form metastatic tumors. Preclinical studies have indicated that the application of antiangiogenic drugs is beneficial in reversing the immunosuppressive microenvironment into an immune-supportive environment and improving the efficacy of vaccine-based antitumor immunotherapy.[36] VEGFA is a pivotal regulator of angiogenesis. The circulating VEGFA levels in patients with GC are associated with increased tumor aggressiveness and poor survival.[37] Interestingly, we found that SPI1+CD68+ TAMs were closely associated with the VEGF pathway via cell–cell communication other than SPI1−CD68+ TAMs, which was further verified in pathological tissue slides. The results suggested that SPI1+CD68+ TAMs were highly enriched around tumor neovascularization. These findings supported that SPI1+CD68+ TAMs affected GC metastasis via angiogenesis.

Immunotherapy, particularly ICIs and adoptive cell transfer therapy, has achieved remarkable clinical progress in cancer treatment.[38 39] Among these approaches, T cells hold a pivotal role in the success of current cancer immunotherapies.[40] However, it is essential to address the issue of T cell exhaustion, a condition marked by the gradual decline in T cell effector functions and self-renewal capacity.[41] T-cell exhaustion is considered one of the pathways

leading to resistance to immunotherapy.[42] PD-1, CTLA4, TIM3, and LAG3 are commonly considered markers of exhaustion in CD8^{+} T cells. Monitoring these markers in CD8^{+} T cells during the treatment process is beneficial for assessing the efficacy of the immunotherapy. It has been shown that macrophages can impede the response to T cell immunotherapy.[43] In our research, the spatial relationship between SPI1^{+}CD68^{+} TAMs and PD-1^{+}CD8^{+} T cells was investigated. The findings revealed that SPI1^{+}CD68^{+} TAMs exhibited a closer association with exhausted T cells in both overall quantity and spatial proximity, as compared with SPI1^{−}CD68^{+} TAMs, indicating that SPI1^{+}CD68^{+} TAMs might participate in the exhaustion of CD8^{+} T cells. Subsequent to being co-cultured with macrophages overexpressing SPI1, the cytotoxic capability of T cells was observed to diminish. Due to the complexity and individual specificity of malignant tumors, achieving better therapeutic effects with a single drug or approach is challenging. The combination and integration of multiple antitumor medicines have shown promising results in various cancers.[44] In particular, the combination of antiangiogenic therapy with immunotherapy demonstrates substantial promise within the domain of oncological treatments.[44 45] For instance, the combination of PD-1/PD-L1 ICIs with antiangiogenic drugs has demonstrated excellent treatment outcomes in hepatocellular carcinoma, renal cell carcinoma, and lung cancer.[46–48] A recent study highlighted that the combination of PD-1 inhibitor atezolizumab with bevacizumab achieved significantly better treatment results in metastatic renal cell carcinoma.[48] Antitumor treatment is increasingly progressing towards the development of combination therapies. In our in vivo experiments, NOD/SCID mice with higher infiltration of SPI1^{+}CD68^{+} macrophages exhibited a stronger response to the combination therapy. Thus, the identification of the macrophage subtypes associated with angiogenesis in this study could provide a novel therapeutic strategy in antiangiogenic strategies in combination with immunotherapy of GC.

ORCID iD
Songcheng Yin http://orcid.org/0000-0002-6156-8797

CONCLUSION

In summary, this study identified SPI1^{+}CD68^{+} TAMs as a novel marker in metastatic GC, which could promote angiogenesis and immunosuppression. SPI1^{+}CD68^{+} TAMs have shown promising effects in combined antiangiogenic and immunotherapy, thereby providing a novel therapeutic strategy in the treatment of GC.[49]

Author affiliations
[1]Digestive Diseases Center, The Seventh Affiliated Hospital Sun Yat-sen University, Shenzhen, Guangdong, China
[2]Guangdong Provincial Key Laboratory of Digestive Cancer Research, The Seventh Affiliated Hospital of Sun Yat-sen University, Shenzhen, Guangdong, China
[3]Department of Gastrointestinal Surgery, Sun Yat-sen Memorial Hospital, Sun Yat-sen University, Guangzhou, Guangdong, China
[4]Department of Gastroenterological Surgery, Peking University People's Hospital, Beijing, China
[5]Department of Gastrointestinal Surgery, the First Affiliated Hospital of Sun Yat-sen University, Guangzhou, Guangdong, China

REFERENCES

1 Sung H, Ferlay J, Siegel RL, *et al*. Global Cancer Statistics 2020: GLOBOCAN Estimates of Incidence and Mortality Worldwide for 36 Cancers in 185 Countries. *CA Cancer J Clin* 2021;71:209–49.
2 Thrift AP, El-Serag HB. Burden of Gastric Cancer. *Clin Gastroenterol Hepatol* 2020;18:534–42.
3 Fares J, Fares MY, Khachfe HH, *et al*. Molecular principles of metastasis: a hallmark of cancer revisited. *Signal Transduct Target Ther* 2020;5:28.
4 Valastyan S, Weinberg RA. Tumor metastasis: molecular insights and evolving paradigms. *Cell* 2011;147:275–92.
5 Li C, Xu X, Wei S, *et al*. Tumor-associated macrophages: potential therapeutic strategies and future prospects in cancer. *J Immunother Cancer* 2021;9:e001341.
6 Zhang Y, Zhang Z. The history and advances in cancer immunotherapy: understanding the characteristics of tumor-infiltrating immune cells and their therapeutic implications. *Cell Mol Immunol* 2020;17:807–21.
7 Mellman I, Coukos G, Dranoff G. Cancer immunotherapy comes of age. *Nature New Biol* 2011;480:480–9.
8 Sharma P, Allison JP. Immune checkpoint targeting in cancer therapy: toward combination strategies with curative potential. *Cell* 2015;161:205–14.

9   Gong J, Chehrazi-Raffle A, Reddi S, *et al*. Development of PD-1 and PD-L1 inhibitors as a form of cancer immunotherapy: a comprehensive review of registration trials and future considerations. *j immunotherapy cancer* 2018;6:8.

10   Powles T, Eder JP, Fine GD, *et al*. MPDL3280A (anti-PD-L1) treatment leads to clinical activity in metastatic bladder cancer. *Nat New Biol* 2014;515:558–62.

11   Li G, Hao W, Hu W. Transcription factor PU.1 and immune cell differentiation (Review). *Int J Mol Med* 2020;46:1943–50.

12   Seki M, Kimura S, Isobe T, *et al*. Recurrent SPI1 (PU.1) fusions in high-risk pediatric T cell acute lymphoblastic leukemia. *Nat Genet* 2017;49:1274–81.

13   Fang Y, Chen W, Li Z, *et al*. n.d. The role of a key transcription factor PU.1 in autoimmune diseases. *Front Immunol*13:1001201.

14   Shen C, Chen M-T, Zhang X-H, *et al*. The PU.1-Modulated MicroRNA-22 Is a Regulator of Monocyte/Macrophage Differentiation and Acute Myeloid Leukemia. *PLoS Genet* 2016;12:e1006259.

15   Liu N, Feng Y, Liu H, *et al*. ATP6V0d2 Suppresses Alveoli Macrophage Alternative Polarization and Allergic Asthma via Degradation of PU.1. *Allergy Asthma Immunol Res* 2021;13:479–97.

16   Li C, Lu C, Gong L, *et al*. SHP2/SPI1axis promotes glycolysis and the inflammatory response of macrophages in Helicobacter pylori-induced pediatric gastritis. *Helicobacter* 2022;27:e12895.

17   Yunna C, Mengru H, Lei W, *et al*. Macrophage M1/M2 polarization. *Eur J Pharmacol* 2020;877:173090.

18   Jiang L, Ping L, Yan H, *et al*. Cardiovascular toxicity induced by anti-VEGF/VEGFR agents: a special focus on definitions, diagnoses, mechanisms and management. *Expert Opin Drug Metab Toxicol* 2020;16:823–35.

19   Locati M, Curtale G, Mantovani A. Diversity, Mechanisms, and Significance of Macrophage Plasticity. *Annu Rev Pathol* 2020;15:123–47.

20   Wynn TA, Chawla A, Pollard JW. Macrophage biology in development, homeostasis and disease. *Nature New Biol* 2013;496:445–55.

21   Orecchioni M, Ghosheh Y, Pramod AB, *et al*. Macrophage Polarization: Different Gene Signatures in M1(LPS+) vs. Classically and M2(LPS-) vs. Alternatively Activated Macrophages. *Front Immunol* 2019;10:1084.

22   Qian BZ, Pollard JW. Macrophage diversity enhances tumor progression and metastasis. *Cell* 2010;141:39–51.

23   Barreby E, Chen P, Aouadi M. Macrophage functional diversity in NAFLD - more than inflammation. *Nat Rev Endocrinol* 2022;18:461–72.

24   Ganesh K, Massagué J. Targeting metastatic cancer. *Nat Med* 2021;27:34–44.

25   Ruffell B, Coussens LM. Macrophages and therapeutic resistance in cancer. *Cancer Cell* 2015;27:462–72.

26   Chistiakov DA, Killingsworth MC, Myasoedova VA, *et al*. CD68/macrosialin: not just a histochemical marker. *Lab Invest* 2017;97:4–13.

27   DeKoter RP, Walsh JC, Singh H. PU.1 regulates both cytokine-dependent proliferation and differentiation of granulocyte/macrophage progenitors. *EMBO J* 1998;17:4456–68.

28   Kueh HY, Champhekar A, Nutt SL, *et al*. Positive feedback between PU.1 and the cell cycle controls myeloid differentiation. *Science* 2013;341:670–3.

29   Shapouri-Moghaddam A, Mohammadian S, Vazini H, *et al*. Macrophage plasticity, polarization, and function in health and disease. *J Cell Physiol* 2018;233:6425–40.

30   Zhang Q, Sioud M. Tumor-Associated Macrophage Subsets: Shaping Polarization and Targeting. *IJMS* 2023;24:7493.

31   Qian F, Deng J, Lee YG, *et al*. The transcription factor PU.1 promotes alternative macrophage polarization and asthmatic airway inflammation. *J Mol Cell Biol* 2015;7:557–67.

32   Zetter BR. Angiogenesis and tumor metastasis. *Annu Rev Med* 1998;49:407–24.

33   De Palma M, Biziato D, Petrova TV. Microenvironmental regulation of tumour angiogenesis. *Nat Rev Cancer* 2017;17:457–74.

34   Majidpoor J, Mortezaee K. Angiogenesis as a hallmark of solid tumors - clinical perspectives. *Cell Oncol (Dordr)* 2021;44:715–37.

35   Fukumura D, Kloepper J, Amoozgar Z, *et al*. Enhancing cancer immunotherapy using antiangiogenics: opportunities and challenges. *Nat Rev Clin Oncol* 2018;15:325–40.

36   Bejarano L, Jordão MJC, Joyce JA. Therapeutic Targeting of the Tumor Microenvironment. *Cancer Discov* 2021;11:933–59.

37   Ferrara N, Gerber HP, LeCouter J. The biology of VEGF and its receptors. *Nat Med* 2003;9:669–76.

38   Postow MA, Callahan MK, Wolchok JD. Immune Checkpoint Blockade in Cancer Therapy. *J Clin Oncol* 2015;33:1974–82.

39   Topalian SL, Drake CG, Pardoll DM. Immune checkpoint blockade: a common denominator approach to cancer therapy. *Cancer Cell* 2015;27:450–61.

40   Wang Z, Wu Z, Liu Y, *et al*. New development in CAR-T cell therapy. *J Hematol Oncol* 2017;10:53.

41   Ma S, Li X, Wang X, *et al*. Current Progress in CAR-T Cell Therapy for Solid Tumors. *Int J Biol Sci* 2019;15:2548–60.

42   Blank CU, Haining WN, Held W, *et al*. Defining "T cell exhaustion." *Nat Rev Immunol* 2019;19:665–74.

43   van Elsas MJ, Labrie C, Etzerodt A, *et al*. Invasive margin tissue-resident macrophages of high CD163 expression impede responses to T cell-based immunotherapy. *J Immunother Cancer* 2023;11:e006433.

44   Zhu S, Zhang T, Zheng L, *et al*. Combination strategies to maximize the benefits of cancer immunotherapy. *J Hematol Oncol* 2021;14:156.

45   Khan KA, Kerbel RS. Improving immunotherapy outcomes with anti-angiogenic treatments and vice versa. *Nat Rev Clin Oncol* 2018;15:310–24.

46   Massari F, Santoni M, Ciccarese C, *et al*. PD-1 blockade therapy in renal cell carcinoma: current studies and future promises. *Cancer Treat Rev* 2015;41:114–21.

47   Horvath L, Thienpont B, Zhao L, *et al*. Overcoming immunotherapy resistance in non-small cell lung cancer (NSCLC) - novel approaches and future outlook. *Mol Cancer* 2020;19:141.

48   Wu M, Huang Q, Xie Y, *et al*. Improvement of the anticancer efficacy of PD-1/PD-L1 blockade via combination therapy and PD-L1 regulation. *J Hematol Oncol* 2022;15:24.

49   Wallin JJ, Bendell JC, Funke R, *et al*. Atezolizumab in combination with bevacizumab enhances antigen-specific T-cell migration in metastatic renal cell carcinoma. *Nat Commun* 2016;7:12624.